

PAPER • OPEN ACCESS

Thermo-hydraulic flow in a sudden expansion

To cite this article: W Jaeger *et al* 2017 *IOP Conf. Ser.: Mater. Sci. Eng.* **228** 012001

View the [article online](#) for updates and enhancements.

Related content

- [Transition between free, mixed and forced convection](#)
W Jaeger, F Trimborn, M Niemann et al.
- [Local symmetry in liquid metals probed by x-ray absorption spectroscopy](#)
Fabio Iesari and Andrea Di Cicco
- [On the effect of the aspect ratio on the mixed convection in a vertical cylindrical cavity with rotating inner wall](#)
A Fichera, M Marcoux and A Pagano

Thermo-hydraulic flow in a sudden expansion

W Jaeger^{1,4}, T Schumm², M Niemann³, W Hering¹, R Stieglitz¹, F Magagnato², B Frohnafel², J Fröhlich³

¹Institute of Fusion and Reactor Technology, Karlsruhe Institute of Technology (KIT), Kaiserstraße 12, 76131 Karlsruhe, Germany

²Institute of Fluid Mechanics, Karlsruhe Institute of Technology (KIT), Kaiserstraße 10, 76131 Karlsruhe, Germany

³Institute of Fluid Mechanics, Technische Universität Dresden, 01062 Dresden, Germany

⁴wadim.jaeger@kit.edu

Abstract. The paper deals with the turbulent flow of liquid metal directed upwards in a vertical channel featuring a backward-facing step. The vertical wall behind the step is heated at various rates thereby inducing forced and mixed convection. Due to the low Prandtl number of liquid metal flow a data basis for this technically relevant flow type did not exist so far. Here, DNS and LES results are presented to provide detailed information about the statistics of the turbulent motion, budgets of turbulent kinetic energy and other quantities. This information is then further used to develop suitable statistical turbulence models capable of properly covering this flow and similar ones, i.e. forced, mixed and free convection of liquid metals. Finally, the paper reports on the construction of an experiment conceived for exactly the same configuration as simulated, with the purpose of close cross validation between the different approaches.

1. Introduction

The thermo-hydraulic behaviour of liquid metal flowing through a vertical backward facing step (BFS) is the subject of this study. The flow separation due to sudden changes of the geometry like the BFS is of crucial importance for the thermo-hydraulic characterisation of various components like heat exchanger, thermal storage containers, manifolds and flow collectors. Such a sudden geometry change paired with an anisotropic heating profile causes flow stratification, stagnation points, re-circulation zones, etc. The resulting unsteady, heterogeneous temperature profile can have a negative impact on the life-time and performance of the aforementioned components, so that reliable prediction of such flows is pressing needed.

The flow over a BFS has been investigated frequently in the past for fluids with a Prandtl number around unity, like water or air. For low Prandtl number fluids like liquid metals (LM), the behaviour differs considerably. The high thermal conductivity of liquid metals induces a separation between the thermal and the viscous boundary layer scale. As a result, the thermal boundary layer is much thicker than the viscous one, making heat conduction the dominant form of heat transfer. Furthermore, the application of LM in engineering is mostly related to turbulent forced convection introducing additional multiscale flow structures for the velocity and temperature field. In addition, buoyancy influences the structure of the flow. Taking all these boundary conditions into account, the turbulent



transport of momentum and energy is challenging, because it necessitates an anisotropic approach for the prediction of the velocity and temperature field. Due to the differences between fluids with low Prandtl number and those around unity a direct transfer of knowledge from one to the other exhibits several deficits. Hence, detailed simulations and experiments with BFS and liquid metal flows are conducted and planned in the near future to address the above mentioned challenges.

A generic BFS is sketched in Figure 1. Iso-thermal investigations are available [1][2], while studies with imposed heat flux [3] are less frequent and studies with mixed convection are very rare [4]. From the technical perspective the following particular problems are to be addressed, among others: identification of the different flow regimes, the transition from forced to mixed to free convection, flow patterns like thermal striping and stratification. From a technical point of view, the prediction of results as a function of dimensionless quantities, like the Péclet number ($Pe = Re \cdot Pr$), the Grashof number ($Gr = g \cdot \beta \cdot (T_s - T_\infty) \cdot D^3 / \nu^2$), the Richardson number ($Ri = Gr / Re^2$) and the Stanton number ($St = Nu / Re$) are desirable.

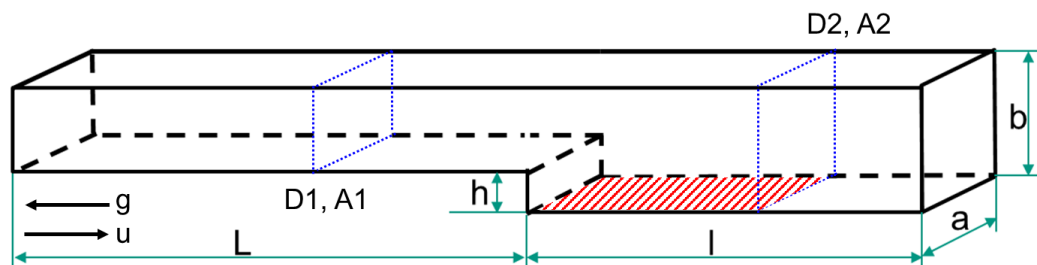


Figure 1. Generic sketch of the backward facing step (BFS) set-up (drawing not to scale). Note that gravity points to the left in this sketch, not downward, i.e. the mean flow is directed upwards.

2. Turbulence-resolving simulations

2.1. Simulation method

This section describes results obtained from simulations representing turbulent flow and buoyancy forces by the unsteady Navier-Stokes equations using the Boussinesq approximation. These equations are solved by a staggered Finite-Volume Method of second order accuracy in space and time [5]. For the lower Reynolds numbers Direct Numerical Simulations (DNS) are conducted resolving all turbulent scales. For the larger Reynolds numbers Large-Eddy Simulations (LES) are performed by means of the σ -model of Nicoud *et al.* [6] to represent the subgrid scales (sgs). Due to the low Prandtl number the smooth temperature field is always fully resolved by the grid employed, and modelling is only required for the dissipation of momentum. A more detailed account on the numerical methods involved can be found in [7] and [8].

2.2. Configuration and grids

For all simulations the configuration is as depicted in Figure 1 and with the inflow condition imposed at section A1. The inflow signal at each grid point of this plane is generated by a separate simulation of the fully developed turbulent flow through a channel of the same cross section and at the same Reynolds number as the main simulation. Most of the simulations are conducted with spanwise periodicity of the solution, the usual approach for DNS and LES in the case of statistically homogeneous conditions in the respective direction. This allows averaging in spanwise direction in addition to time averaging and reduces computational requirements substantially. Two further simulations are conducted assuming sidewalls to assess the impact of secondary flows on the obtained results. Their impact is larger the shorter the distance is between them, so that a width of $a = h$ has been chosen to provide information about what could be termed a case of large comparatively

alteration with respect to the spanwise homogeneous case. This distance is smaller than planned for the experiments discussed below to create a kind of upper bound for the impact of this feature. A no-slip condition is imposed on all solid walls and a convective outflow condition in the outlet plane at a distance of $l = 30h$ behind the step is considered, with a heated section of $20h$ in streamwise extension. The temperature is set to $T_{in} = 150^\circ\text{C}$ at the inlet and a transport equation is solved for the non-dimensional temperature rise $\theta = (T - T_{in})/\Delta T$. All solid walls are assumed adiabatic, except the wall behind the step, where constant heat flux \dot{q} is imposed. The characteristic temperature difference ΔT is obtained from the imposed heat flux density $|\dot{q}| = \lambda \cdot \Delta T/h$. For all cases a Prandtl number of $Pr = 0.0088$ is assumed corresponding to that of liquid sodium at the chosen inlet temperature. Several cases for the Reynolds and Richardson numbers based on the step height h and the bulk velocity at the inlet U_b have been computed. The flow domain is discretized with Cartesian grids refined towards the walls and stepwise adapted for each case to resolve all boundary layers. Such an approach results in 40 up to 650 million cells, depending on the physical parameter magnitude.

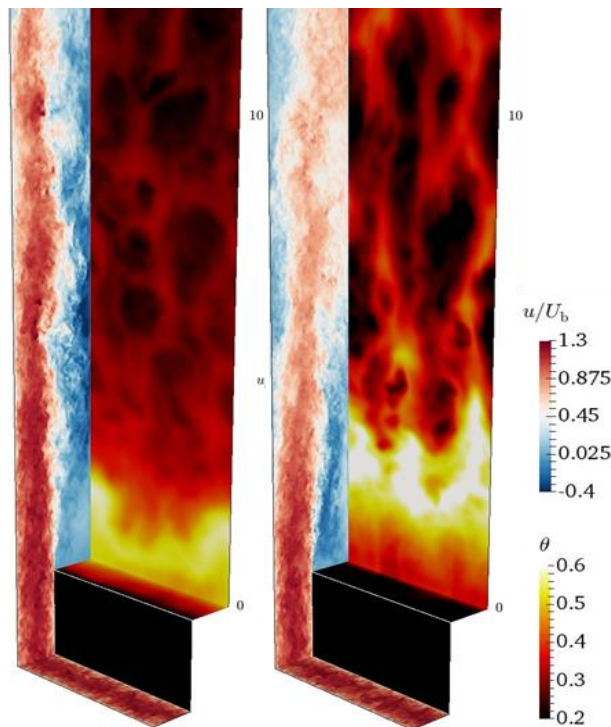


Figure 2. Overview of instantaneous LES dimensionless velocities and temperatures for $Re_h = 20000$ with $Ri = 0.0$ (left) and $Ri = 0.2$ (right). The streamwise velocity is shown on the inlet plane and at the periodic boundary. The step and the heated wall are colored by instantaneous temperature. Note the different scales.

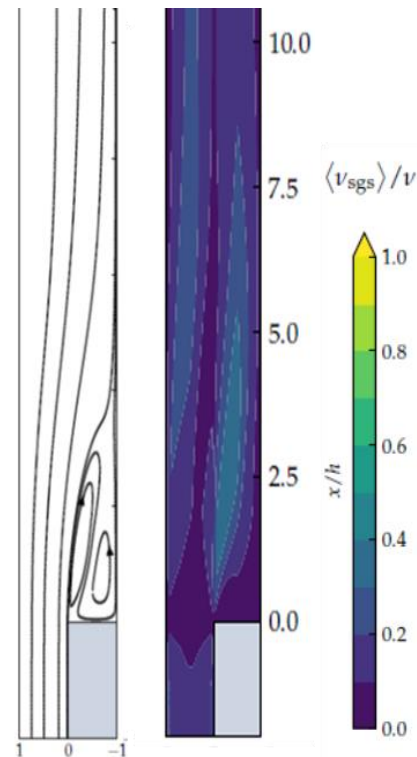


Figure 3. Streamlines of the main flow (left) and average subgrid-scale viscosity compared to the molecular viscosity (right) for the flow with $Re_h = 20000$ and $Ri = 0.2$.

2.3. Results for spanwise homogeneous flow

The numerical method has been validated with a DNS of a non-isothermal air flow over a BFS for $Re_h = 4805$, $ER = b/(b-h) = 1.5$ from [3], and the impact of temperature-dependent fluid properties of liquid sodium have been found to be marginal [7]. In [8], the flow of LM has been simulated with the same expansion rate for $Ri = 0.338$, comparing it to the non-buoyant flow with $Ri = 0.0$. Detailed one-

point statistics, Nusselt number and wall friction profiles have been provided. These data are then used for model assessment in [9]. Selected results appear in Figure 6 - Figure 8 below.

The experiment described in Section 4. is supposed to be run with larger expansion ratio, $ER = 2$, so that DNS with this value and $Re_h = 10000$ have been performed varying the Richardson number from $Ri = 0.0$ to $Ri = 0.4$. On one hand, these data are used to assist in the construction of the experiment, but most of all they are aiming at model validation [9] as reported below in Section 3.3. and 3.4. For these cases, not only one-point statistics of velocity and temperature are determined, but also two-point correlations and all budget terms for the fluctuating quantities.

For even larger Reynolds numbers, a DNS demands excessive computational requirements, so that LES have been executed for $Re_h = 20000$ and $Re_h = 40000$ on grids of 420 to 549 million cells. Again, all one-point statistics and budget terms have been determined. An impression of these simulations is provided by Figure 2 and Figure 3, where instantaneous flow data for $Re_h = 20000$ are shown together with the streamlines of the mean flow for $Ri = 0.2$. It is visible that the upward buoyancy force accelerates the flow along the wall behind the step entraining the fluid towards this side resulting in a deceleration close to the straight wall. The ratio of the mean sgs viscosity to the molecular viscosity is reported as well. It is below 0.5 in most of the domain, indicating that the sgs model has an impact on the flow but does not dominate the dissipation. For the higher Reynolds number, the values are about twice as large (not shown here), so that in this case the model contributes sizably, as to be expected. Furthermore, the ratio is slightly larger for $Ri = 0.0$ than for $Ri = 0.2$ since the gradients of the mean flow are stronger without buoyancy which deviates the mean flow towards the heated wall.

2.4. Results for the step with sidewalls

An overview of the flow with sidewall at $Re_h = 10000$ without buoyancy is illustrated in the left picture of Figure 4 showing streamlines of the mean flow starting close to the wall upstream of the step and points between the channel wall (dark green) and points in the center (dark brown). Secondary flow of the first kind results from curvature of the mean flow behind the step. This secondary flow entrains streamlines close to the sidewalls towards the channel center within the recirculation zone and outwards in the reattachment region. On top of this effect, secondary flow of the second kind also affects the velocity field, as visible, for instance, in the inflow section where one of the depicted streamlines near the side wall is advected away from the heated wall. In the mixed convection case, addressed in the right picture of Figure 4, secondary flow of the first kind is also present in the recirculation zone but has no visible effect on the streamlines near reattachment. Here, the selected streamlines concentrate in the channel center at the heated wall, as a result of both the development of the wall jet and the effect of the secondary flow affecting the mean flow in this part of the domain.

The mean wall shear stress at the heated wall illustrates the substantial difference between the two regimes. A clear dependence on the distance from the side wall is visible for $Ri = 0.0$ and thick boundary layers at the side walls are present downstream of reattachment. For $Ri = 0.2$ the wall shear stress on the heated wall varies less in the channel center in spanwise direction and thinner boundary layers at the sidewalls are found.

Figure 5 shows profiles of the mean streamwise velocity component in the channel center for the two Richardson numbers addressed in Figure 4. Furthermore, these data are compared to the corresponding values for the cases with the same Reynolds number and spanwise periodicity. For both Richardson numbers, the difference between the cases with and without sidewalls are moderate. The main difference is a slightly higher velocity in the center for the case with sidewalls, as expected, since the bulk flow rate is assumed the same in both cases. This somewhat shifts the center of gravity of the velocity profile but does not introduce qualitative changes. The second graph in Figure 5 shows the turbulent kinetic energy. Here, the same observations can be made. Far downstream of the step, around $x/h = 12$ and 15 , however, the results with and without sidewalls differ by a factor of 2 and more, which is substantial, and results from the differences in the secondary flow and the attenuating effect of the additional walls. All three normal stresses (not shown here) contribute to this behavior.

For the mixed convection cases, the decrease downstream of reattachment is smaller than for $Ri = 0$. In the recirculation zone substantial deviations between periodic case and side wall case are observed near the heated wall resulting from the substantial difference in the secondary flow.

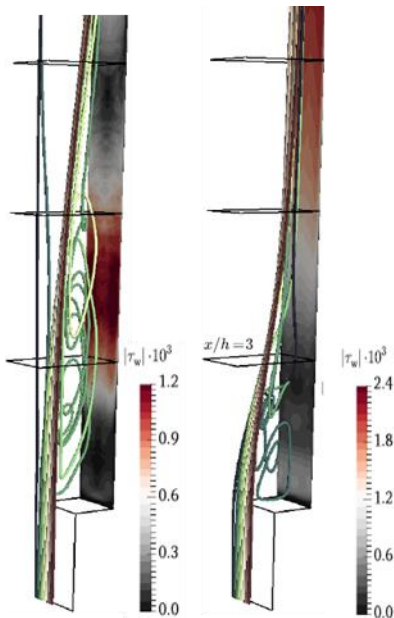


Figure 4. Selected streamlines and absolute value of the wall shear stress at the heated wall for the flow over the step with side walls with $Ri = 0.0$ (left) and $Ri = 0.2$ (right).

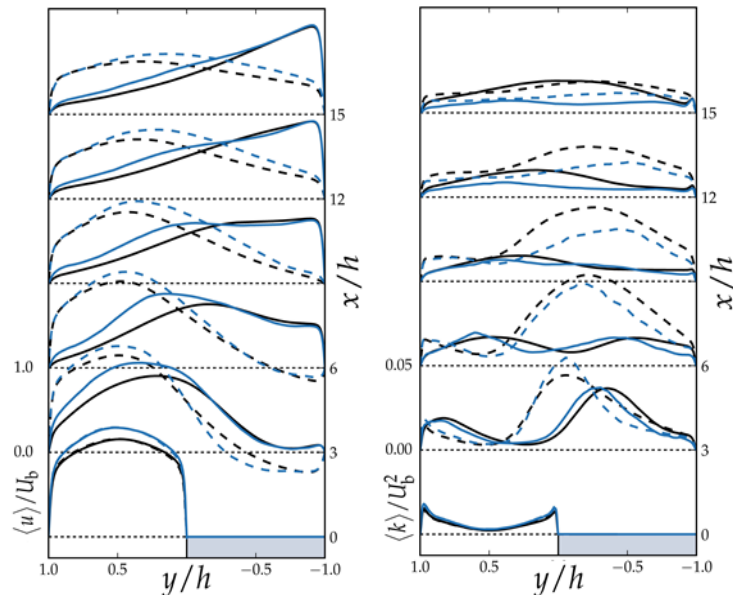


Figure 5. Mean streamwise velocity and turbulent kinetic energy at the channel center for the cases with side walls (light blue) in comparison with results of the periodic cases (black). Dashed lines: $Ri = 0.0$. Solid lines: $Ri = 0.2$.

3. Turbulence and heat flux modelling

3.1. Validation of turbulence and heat flux models for the BFS

The turbulent flow over a BFS is a well-known generic test case for turbulence models, as it features an adverse pressure gradient, flow separation and the development of a boundary layer. Additionally, due to the complex flow structure, the Reynolds analogy, describing the similarity between the viscous and the thermal field, is not valid [10]. Also for liquid metals, the Reynolds analogy cannot be assumed, as due to the high thermal diffusivity (α_t) a constant relation between the Reynolds shear stresses and turbulent thermal diffusion is not given. Consequently, the correct prediction of the heat transfer poses a challenge and needs special attention in terms of heat flux modelling.

Investigations of the heat transfer downstream of a BFS revealed, that the expected reattachment length is a good criterion to select turbulence models. During the investigation, two different cases with changing reattachment lengths are considered.

One major finding of previous investigations is that a lower expansion ratio, ER, features smaller reattachment lengths and vice versa [11][12][13][14]. Within the present investigation this finding is confirmed, however, for the case with $ER = 2$, a larger reattachment length than the one reported by [14] is found. The difference is attributed to the different boundary layer conditions at the separation point. From the turbulence modelling point of view, the estimation of the reattachment length seems to be important for the choice of the turbulence model. Linear k - ϵ -models (model of Abe, Kondoh and Nagano [15] – AKN – and the one of Launder Sharma [16] in conjunction with the Yap correction

term [17]–LSY) seem to be better suited for predicting the flow structure at smaller reattachment lengths. Contrary, the $k-\omega$ based turbulence models (model of Wilcox [18] – SST – and Hellsten [19]), as well as the non-linear v^2-f model of [20], in combination with Durbin’s realisability constraints [21], (V2F) show a better agreement with the data of [22][23] for the simulations featuring a larger reattachment length. Therefore, the results of the different simulations are discussed separately. The turbulent heat fluxes are modelled with the Single-Gradient-Diffusion-Hypotheses (SGDH), where the turbulent diffusion of heat (α_t), is computed by two different models, firstly the local correlation of Kays [24] and secondly the two equation heat transfer model of Manservigi and Menghini [25]. The AKN model is coupled with the two equation model of [25] and is referred to as MM, while all other models use the Kays correlation for the computation of the turbulent heat fluxes.

3.2. Forced convective flow over a BFS with $ER = 1.5$

The turbulent flow over a BFS with $ER = 1.5$ and $Re_h = 5000$ is discussed. As mentioned above, the flow features a short reattachment length ($x/h = 6.9$), shown in Figure 6. It can be noticed, that the AKN model and the LSY model show a good agreement with the data of [8] in respect to the reattachment length, whereas the other models over-estimate x . The differences in the reattachment length can be attributed to the discrepancies in the shear stress profiles predicted by the different models as illustrated in Figure 7. A good agreement between the numerical data of [8] and all RANS results is achieved for the mean velocity profiles, as well as for the turbulent kinetic energy, similar as in [26]. For the LSY model, the fluid experiences the step at a later position, resulting in a sharp edge in the velocity at $x/h = 1.0$, as discussed in [26].

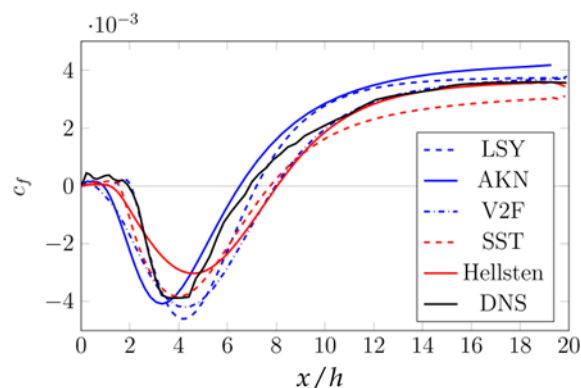


Figure 6. Skin friction distribution downstream of the separation point for $Re_h = 5000$.

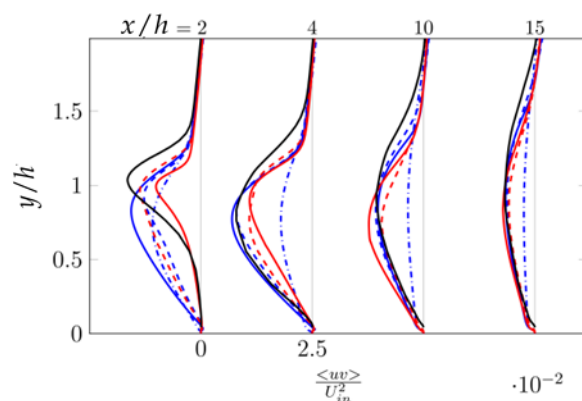


Figure 7. Comparison of the Reynolds shear stress at several positions downstream of the separation point (legend as in Figure 6).

A good prediction of the momentum field is only a pre-requisite for a correct thermal field according to the Reynolds analogy deficit in low Prandtl number fluids. This statement is supported by the large scatter in the Stanton number profiles predicted by the different models shown in Figure 8. The LSY model in combination with the Kays correlation provides the best prediction compared to the data of [8], see also [9], [26]. The other models, using the same correlation for the turbulent heat fluxes, exhibit reduced Stanton number profile. The V2F model predicts a significantly lower Stanton profile than the DNS data, as shown in Figure 4. This behavior is expected, as the Kays correlation is based on the correct prediction of the eddy viscosity. Thus, the considerable under-estimation of the shear stresses shown in Figure 7 implies lower turbulent heat fluxes compared to the other models. The MM model is not capable to predict the corner eddy in the velocity field, which influences the

thermal prediction close to the step, indicated by a lower St . This shortcoming leads to an overestimation of Stanton number for the region of the recirculation zone. After the reattachment point the computed Stanton number converges towards the one of the DNS. That demonstrates, that the correct predictions of the flow physics after the separation point, like the existence of the corner eddy, is of great importance for the computation of the heat transfer, also for fluids with a very large thermal diffusion. To understand the contribution of the eddy diffusivity of heat to the total thermal transport at the given Reynolds and Prandtl number, the ratio of turbulent and molecular diffusion is illustrated in Figure 9. In the near wall region, the effect of turbulent diffusivity is very small and can be neglected. Further above, nearly half a step height away from the wall, its influence is increasing up to 50 % of the molecular diffusion at $x/h=10$. Further downstream of the reattachment point, the area affected by turbulent diffusion is expanding and the peak is shifting away from the heated wall towards the duct center.

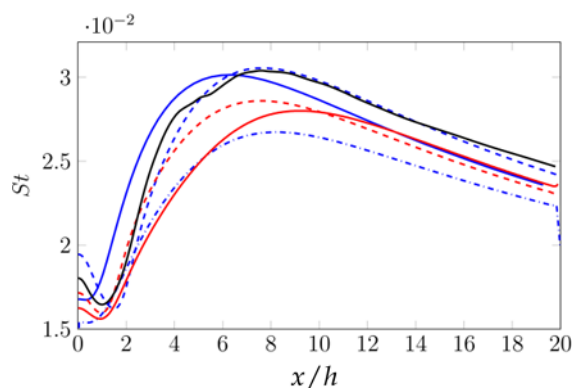


Figure 8. Stanton number distribution downstream of the separation point for $Re_h = 5000$ (legend as in Figure 6).

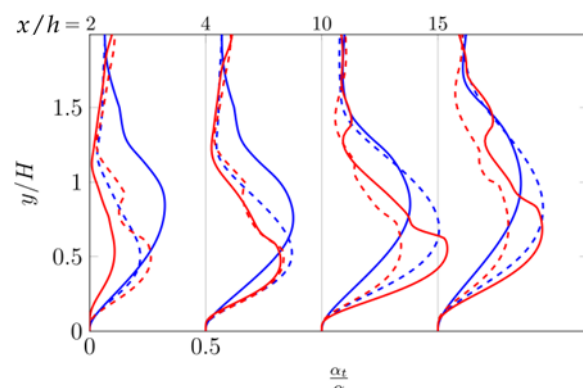


Figure 9. Comparison of the ratio of eddy to molecular diffusivity of heat at several positions downstream the separation point (legend as in Figure 6).

3.3. Forced convective flow over a BFS with $ER = 2.0$

As mentioned, the reattachment length for a turbulent flow over a BFS increases, compared to the previous case. Therefore, the $k-\omega$ models show a better agreement with the DNS data of [22], [23] in terms of the skin friction distribution, see Figure 10. Surprisingly, for $Re_h = 10000$, nearly all models over-predict the heat transfer within the recirculation zone. This difference is caused by the low inflow Reynolds number together with the high expansion ratio, leading to reduced shear stresses downstream the separation point and thus reduced turbulent heat fluxes compared to the previous case. The reduced contribution of the turbulent heat fluxes on the global heat transfer is supported by a simulation assuming that the thermal diffusivity is zero, shown in Figure 11. There, the Stanton number profile collapses with DNS data up to $x/h = 3$. Further downstream, the influence of the turbulent heat fluxes is enhanced and the temperature transport within the fluid increases. Thus, the Stanton number of the DNS data grows further.

3.4. Buoyancy aided mixed convective flow over a BFS with $ER=2.0$

The influence of buoyancy is investigated by means of RANS simulations for the turbulent flow over a BFS at $Re_h = 10000$ with $ER = 2$ [27]. The goal is to verify fast and simple methods for complex flows and thermal structures. Therefore, only the linear model of LSY in conjunction with the Kays correlation is used. Similar to investigations of [33], who reported an increase in heat transfer for buoyancy-aided mixed convection for liquid sodium with $Pr = 0.005$, a larger heat transfer is found for the turbulent flow of sodium over a BFS with a slightly larger molecular Prandtl number of $Pr = 0.0088$ as shown in Figure 12. The investigation reveals that buoyancy contributes in accelerating

the fluid close to the heater. The incoming flow is diverted towards the heated wall more strongly for the mixed convection cases than for the forced convection cases. Subsequently, the flow impinges on the heater earlier with increasing influence of buoyancy. The impingement leads to a higher heat transfer as shown in Figure 12.

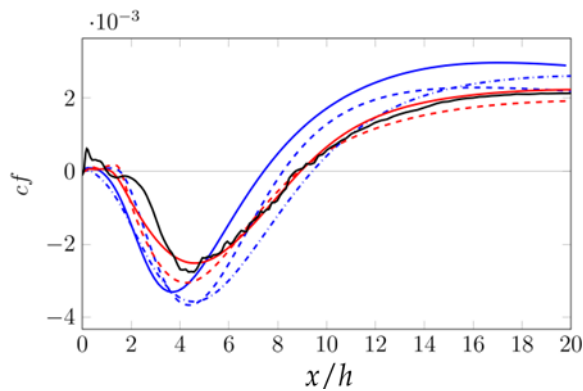


Figure 10. Skin friction distribution downstream of the separation point for $Re_h = 10000$ (legend as in Figure 6).

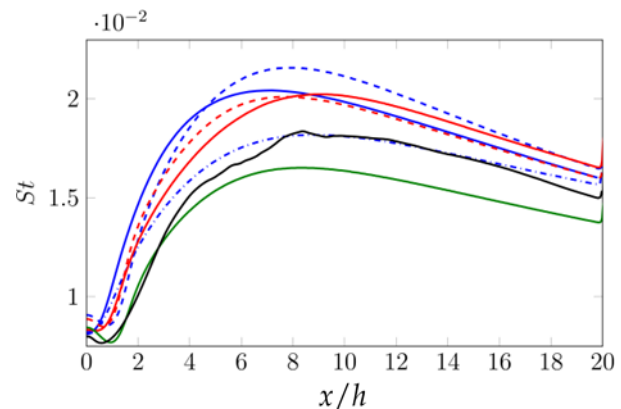


Figure 11. Stanton number distribution downstream of the separation point for $Re_h = 10000$ (legend as in Figure 6 - the green line corresponds to the simulation with $\alpha_t = 0$).

Towards the end of the heater, a decrease in c_f is found for $Ri > 0.2$. This decrease is attributed to the strong increase in turbulent shear stresses, which counter-acts the buoyancy force and decelerates the fluid, thus reducing the near wall velocity gradients as reported in [9], [26]. The influence of eddy diffusion of heat increases further downstream, as the turbulence is generated by the high shear stresses. Nevertheless, the acceleration of near wall velocity is responsible for the enhanced heat transfer found for increasing buoyancy.

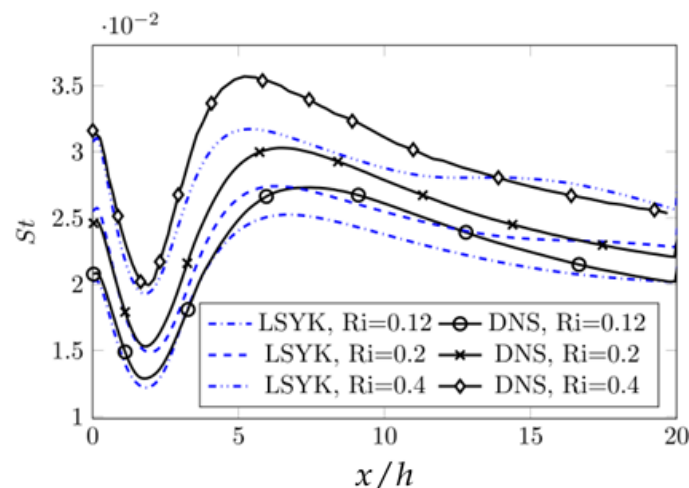


Figure 12: Comparison of the Stanton number distribution downstream of the separation point for $Re_h = 10000$ at different Richardson numbers with Ref. [23].

4. Preparation of a BFS experiment

4.1. The BFS design

To support the numerical investigations an experiment set-up for the BFS is currently under construction. The BFS test section is divided into four parts, as depicted in Figure 13. The first section is the inlet section. It is basically the transition region from circular cross section to rectangular cross section. Furthermore, it contains perforated plates for flow rectification. The second section is the rectangular part of the BFS. A commercially available duct with rounded corners is used. The main reason is that, first of all, for engineering applications commercially available components would be used rather than expensive single-part products. Second, the ducts with rounded corners have only one welded seam. A construction of a rectangular duct with sharp corners made from simple steel plates would require several welded seams. This is of disadvantage for the dimensional accuracy due to the large heat input. Furthermore, wire and sinker EDM are very expensive for the envisaged lengths of ducts. The commercially available ducts prove to be very accurate and the welded seam satisfies the requirements for, e.g., safety. Detailed studies are performed to investigate the difference between channels with sharp 90° corners and rounded corners [28]. The outcome is that no difference in the general behavior exists between the two flows. In the present case, the rectangular section of the BFS has a length of 3600 mm and an internal cross section of 90×40 mm. The outer radius of the corners is 2 times the wall thickness, which is 5 mm. With this cross section, the undisturbed length of the rectangular section is around 65 hydraulic diameters and equals $x/h = 72$. Studies related to the entrance length effect of liquid metal cooled rod bundles and circular ducts show that such an entrance length is sufficient to provide a hydraulically developed flow at the step [29]. The third section is the quadratic section of the BFS. It is 2000 mm long and has an internal cross section of 90×90 mm, which equals to $x/h = 40$. The wall thickness and the radius of the rounded corners are identical to the rectangular section. The inside surface and the welded seam will be mechanically treated to guarantee a homogeneous surface. The last section, section four is the outlet section, which is the transition from a quadratic cross section to a circular cross section. The presented approach limits the number of welds, which may have a negative impact on the flow.

To minimize the thermal losses during the operation, the BFS is equipped with a trace heating system and with a thermal insulation. The thermal insulation is made of a 100 mm thick rock wool layer (approximately thermal conductivity = $0.0038 \text{ W/m}\cdot\text{K}$)

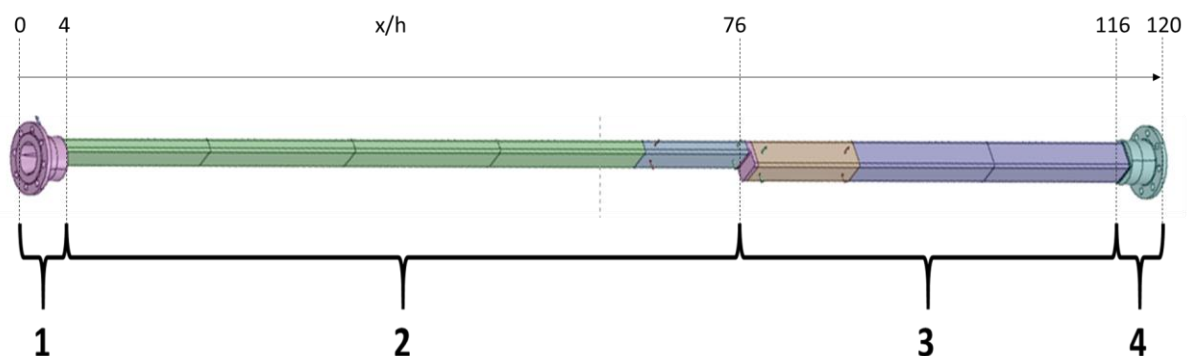


Figure 13. BFS test section (1 - inlet section, 2 - rectangular section, 3 - quadratic section, 4 - outlet section)

For the present BFS temperature and velocity measurements will be taken globally and at discrete local positions. First of all, the temperature of the heated wall, indicated by the red shaded area in Figure 1, and the fluid temperature above the heated section at the centerline are measured using sheathed thermocouples. With the knowledge of the temperature dependent thermo-physical properties

and the given heat flux density the heat transfer coefficient and also the Nusselt number can be derived. Second, traversable permanent magnet probe sensors (PMP) are foreseen to measure the temperature and the velocity at pre-defined positions, to identify the point of reattachment of the flow after the separation. Furthermore, the provision of temperature and velocity field data aims to provide input for CFD, LES and DNS simulation. Depending on the configuration of the permanent magnetic probe the turbulent heat fluxes on a local level can be evaluated. A detailed description of permanent magnet probe sensors can be found in [30][31][32].

Given the KASOLA corner data, the developed BFS test section is capable to cover the following parameter range: $5000 \leq Re \leq 10^6$; $0.005 \leq Pr \leq 0.008$; $25 \leq Pe \leq 8500$. Depending on the heating scheme and the pump operation, a Richardson number in the order of 1.0 can be realized. Thereby, the entire Richardson and Péclet number regime from purely buoyancy driven flow to pure convective flow can be covered. Additionally, the developed design allows for an exact determination of the transitional domains.

4.2. The KASOLA facility

The BFS test section will be integrated into the KASOLA (KArlsruhe SOdium LAboratory) facility, being illustrated in Figure 14.

The KASOLA facility is a flexible, medium size, loop type experimental facility. The facility is sheltered by a cylindrical steel containment with a height of 12 m and a diameter of 8 m. The only exception is the sodium storage tank, which is located in an underground storage outside the steel containment. The storage tank has a sodium volume of 7 m³. The KASOLA facility has a maximal electrical consumption of 2 MW (trace heating, experimental heating, pump, etc). The basic loop contains the following components: Two test section ports, a magneto-hydrodynamic pump, the sodium-air heat exchanger, a magnetic flow meter, an expansion tank and the sodium precipitator. The developed length of the basic loop equals 37 m. The piping between the components is made of DN 100 stainless steel pipes. During operation roughly 1 m³ of sodium is in the loop. Furthermore, the basic loop is equipped with several valves for operational and safety purposes. In a by-pass line to the basic loop, a second flow meter, Coriolis type, and a cold trap for sodium purification are installed. The whole facility, basic and by-pass loop are enveloped with a trace heating system to prevent the sodium from freezing. The sodium storage tank and the expansion tank are under an Argon atmosphere. To remove the energy dissipated into the sodium an air cooled heat-exchanger is integrated and in the cold trap three separate air cooling circuits are installed.

For a maximum of operational and experimental flexibility, two test section ports are installed. The first port is foreseen to house experiments related to duct and pipe flow like the BFS. With a total free length of six meter the installed test section allows additional flexibility for the study of different flow phenomena. The second test port is related to the investigation of thermal storages. A thermocline storage tank with a movable separating plate will be installed to investigate the feasibility of sodium as a heat transfer and storage fluid for concentrated solar power applications. The tank has a volume of about 0.5 m³ and a storage capacity of 50 kWh. The KASOLA configuration allows a simultaneous operation of both test loops.

The magneto-hydrodynamic pump can deliver a maximal volume flow rate 150 m³/h (37.65 kg/s) and a maximal relative pressure head of 6 bar. The maximal volume flow rate corresponds to a Reynolds number of approximately 10⁶ for the quadratic test section of the BFS. The operational temperature of the facility is in the range of 150 to 550°C. For the sodium cooling, the sodium-air heat exchanger has a maximal thermal duty of 970 kW. The sodium-air heat exchanger can be operated on the air side with an air flow rate of 4.4 kg/s and a maximal temperature increase of 210°C. Because KASOLA is foreseen to operate anywhere between 150 and 550°C an expansion tank is installed at the top of the basic sodium loop.

The operation of the facility is realised by two automatic Programmable Logic Controller units. One is for the general operation of the loop, while the other is connected to the trace heating system. In addition, an automatic shut-down system is installed.

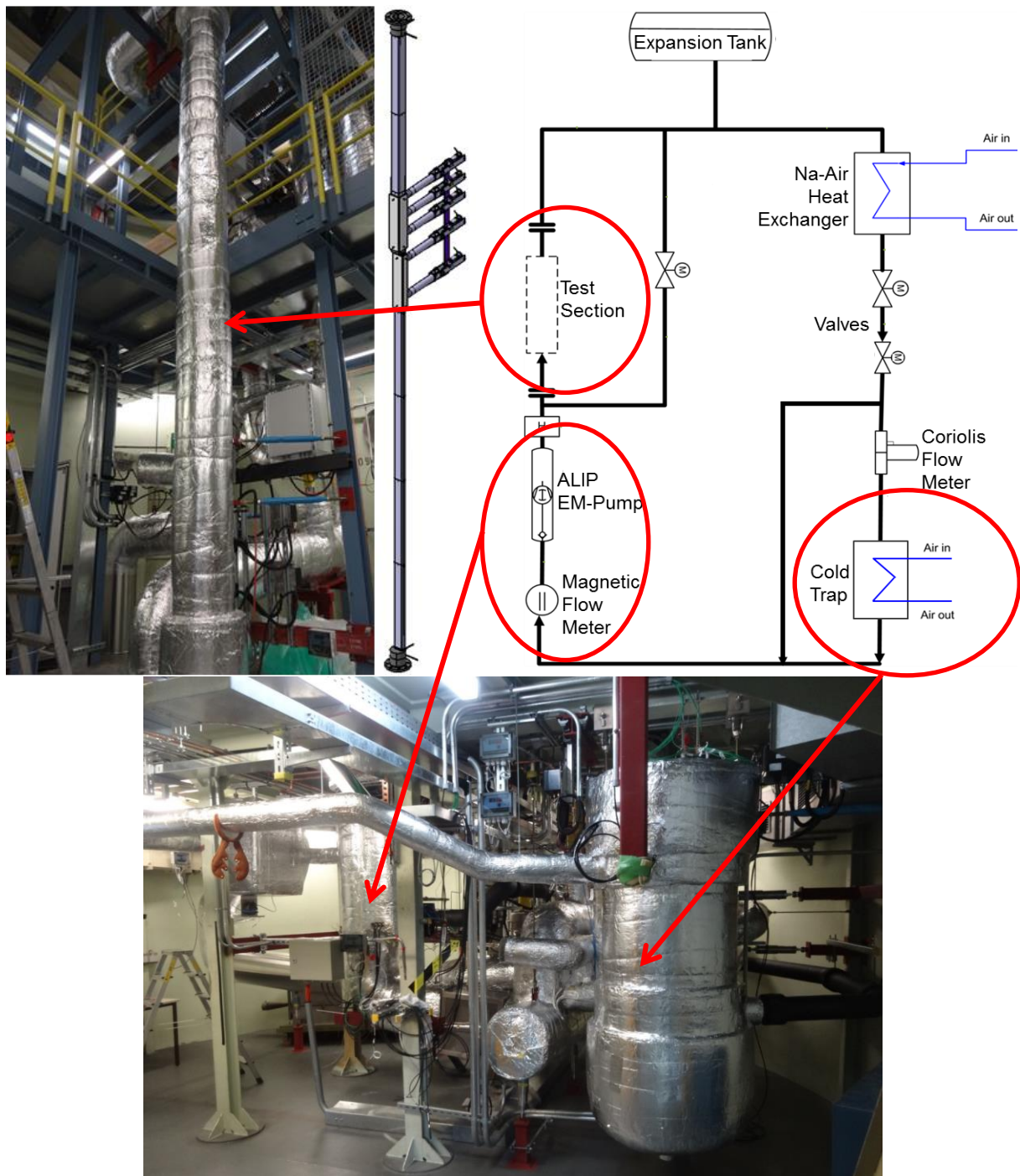


Figure 14. Impressions of the KASOLA facility

The KASOLA loop is connected to an Argon system. This system is used to avoid sodium oxidation, to maintain a pre-defined system pressure and to assist during the filling and evacuation of the main components of the KASOLA facility include:

- Storage tank: 8 m³ with 7 m³ of sodium and argon cover;
- Expansion tank: 0.3 m³ and argon cover;

- Stainless steel piping system: DN 100, PN 16, up to 550°C;
- Magneto-hydrodynamic pump: 75 kW, 150 m³/h (37.65 kg/s);
- Cold trap: Sodium purification;
- Sodium precipitator: Protection against sodium leakage into the argon system;
- Trace heating: 40 kW for the loop, 32 kW for the storage tank;
- Thermal insulation: Rock wool 100 mm piping, 200 mm thermal storage;
- Magnetic flow meter: Operation;
- Coriolis flow meter: Calibration and control;
- Sodium-air heat exchanger: ~ 1 MW;
- 2 test section ports: 1 for BFS, 1 for thermal storage;
- Containment: Steel cylinder, 12 m high, 8 m in diameter;

The KASOLA facility is currently in the commissioning phase (until August 2017). First general experiments are foreseen with the basic loop (until March 2018) and experiments with the BFS are foreseen to take place afterwards (beginning April 2018).

5. Summary

This article describes numerical and technical developments to investigate the vertical backward facing step (BFS) problem for a low Prandtl number medium such as liquid metals, appearing in several technical applications.

In this context a quasi-exact solution of the flow has been developed, verified and validated by means of a turbulence resolved modelling of the flow problem based on a Direct numerical simulation (DNS) or a corresponding DNS to serve as a reference solution. In this context not only the mean fluid wall interface temperatures are developed to provide an indication for the test-sectional set-up of the BFS experiments, but rather to describe the exact transport quantities for the momentum and temperature field wall normal to the heated section along the entire heated length to identify stagnation points and recirculation domains peculiar to any technical design. Since this approach demands excessive computational power, this solution formed the pre-requisite for a numerical computations relying on turbulence models providing a prediction of technically relevant parameters as the fluid/wall interface temperature (or Nusselt number) at a substantially faster computational speed. Several turbulence models have been analysed and compared in the budget terms to the DNS data provided. Thereby, it turns out no superior turbulence models is currently available to describe all potential developing flow and temperature distributions adequately. Most essential is however, that already the momentum field is correctly depicted to execute a reliable prediction of the thermal field, which excludes some of the conventionally used turbulence models.

Based on the obtained numerical data a BFS test-sectional lay-out with a corresponding instrumentation has been developed to be integrated in the KASOLA facility aiming either to verify the model calculations or to elucidate drawbacks of currently existing models requiring a more complete model description. Moreover, the set-up in the KASOLA facility is not only targeting a model validation but also to provide a data basis for parameter regimes also in the near future hardly numerically accessible. Unfortunately, due to technical constraints the successful operation could not be achieved within the project duration.

Acknowledgments

The financial support of the Helmholtz Alliance “Liquid Metal Technologies – LIMTECH” is gratefully acknowledged.

References

- [1] Le H, Moin P and Kim J 1997 *J. Fluid Mech.* **330** 349-74
- [2] Barri M and Andersson H I 2011 *J. Fluid Mech.* **665** 382-417

- [3] Avancha R V R and Pletcher R H 2002 *Int. J. Heat Fluid Flow* **23** 601-14
- [4] Abu-Mulaweh H I, Chen T S and Armaly B F 2002 *Int. J. Heat Fluid Flow* **23** 758-65
- [5] Kempe T and Fröhlich J 2012 *J. Comput. Phys.* **231** 3663–3684
- [6] Nicoud F, Toda H B, Cabrit O, Bose S and Lee J 2011 *Phys. Fluids* **23** 085106
- [7] Niemann M and Fröhlich J 2014 *Proc. Appl. Math. Mech.* **14** 659-660
- [8] Niemann M and Fröhlich J 2016 *Int. J. Heat Mass Transfer* **101** 1237-50
- [9] Schumm T, Niemann M, Marocco L, Magagnato F, Frohnäpfel B and Fröhlich J 2015 *Proc. of 8th Int. Symp. on Turbulence, Heat and Mass Transfer* vol 1 ed K Hanjalic et al (New York, Begell House Ind.)
- [10] Vogel J C and Eaton J K 1985 *J. Heat Transfer* **107(4)** 922-9
- [11] Eaton J K and Johnston J P 1980 Rept MD-39, Dept of Mech Eng, Stanford University, Stanford, CA
- [12] Durst F and Tropea C 1981 *Proc. 3Rd Symp Turb Shear Flows* (Davis)
- [13] Adams EW and Johnston J P 1988 *Exp. Fluid* **6** 493-9
- [14] Nadge P M and Govardhan R N 2014 *Exp. Fluids* **55(1)** 1657
- [15] Abe A, Kondoh T and Nagano Y 1994 *Int. J. Heat Mass Transfer* **37** 139-51
- [16] Launder B E and Sharma B I 1974 *Letters in Heat and Mass Transfer* **1** 131-7
- [17] Yap C R 1987, Ph.D. Thesis (Manchester University England)
- [18] Menter F 1994 *AIAA J* **32** 1598-605
- [19] Hellsten A 2005 *AIAA J* **43** 1857-69
- [20] Davidson L, Nielsen P and Sveningsson A 2003, *Proc. of 8th Int. Symp. on Turbulence, Heat and Mass Transfer* **4** 577-84
- [21] Durbin P A 1996 *Int. J. Heat Fluid Flow* **17** 89-90
- [22] Niemann M and Fröhlich J 2015 *Proc. Direct and large-Eddy Simulation* **10**
- [23] Niemann M and Fröhlich J 2016 *Proc. Int. Symp on Eng. Turb. Mod. And Meas.* **11**
- [24] Kays W M 1994 *J. Heat Transfer* **116** 284-95
- [25] Manservigi S and Menghini F 2014 *Int. J. Heat Mass Transfer* **69** 312-326
- [26] Schumm T, Frohnäpfel B and Marocco L 2016 *J. Phys.: Conf. Ser.* **745** 032051
- [27] Schumm T, Frohnäpfel B and Marocco L 2017 *Heat Mass Transfer* (in press)
- [28] Jaeger W, Schaub Hahn T, Hering W, Otic I, Shams A, Oder J and Tiselj I 2017 *Proc Int. Topical Meeting on Nuclear Reactor Thermal Hydraulics* **17**
- [29] Jaeger W 2017 *Heat Mass Transfer* **53(5)** 1667-84
- [30] von Weissenfluh T 1985 *Int. J. Heat Mass Transfer* **28(8)** 1563-75
- [31] Knebel J U and Krebs L 1994 *Exp. Therm Fluid Sci.* **8** 135-48
- [32] Kappulla R, Sigg B, Horanyi S and Hudina M 2000 *Exp. Therm Fluid Sci.* **20** 115-36